Role of different nitrogen functionalities on the electrochemical performance of activated carbons

Tomás Cordero-Lanzac, Juana M. Rosas, Francisco J. García-Mateos,
Juan J. Ternero-Hidalgo, José Palomo, José Rodríguez-Mirasol*, Tomás Cordero

Universidad de Málaga, Andalucía Tech., Departamento de Ingeniería Química, Campus de Teatinos s/n, 29010, Málaga, Spain.

*Corresponding author: mirasol@uma.es. Tel: +34 951 952 385

ABSTRACT

Different oxidation, reduction and thermal methods are used for selectively obtaining each of the most common surface nitrogen groups (almost isolated) on the surface of a phosphorus-containing activated carbon (ACP), and their electrochemical performance are analyzed. Nitro- and amino- containing activated carbons show defined pseudocapacitive peaks, characteristic of redox processes, which can be associated to the formation of hydroxylamino groups (observed by means of XPS). Condensed structures of nitrogen, such as pyridinic and pyrrolic, additionally improve the ionic diffusion on the carbonaceous structure, increasing the specific capacitance of the carbon electrode up to 317 F g^{-1}. The formation of poly(amido-amine) chains on ACP surface leads to an activated carbon with poor textural properties (A_{BET} = 43 m^2 g^{-1}) but surprisingly high surface capacitances (ca. 3256 mF m^{-2}) attributed to an enhancement of the carbon conductivity. Some of the activated carbons are submitted to a severe thermal treatment at 900 ºC, yielding carbons with a developed porous texture, stable surface phosphorus groups and an increased proportion of quaternary nitrogen surface species. These activated carbons exhibit a faster development of the electric double layer, due to the more ordered carbon planes and the presence of charged functional groups.

1. Introduction

Activated carbons are usually prepared from waste or lignocellulosic raw materials in an environmentally attractive process [1,2]. They are traditionally used as adsorbent or catalyst support due to their surface properties, with elevated surface areas and pore volumes (mainly micropores) [3,4]. The recent advances in electrochemistry and the increasing knowledge on carbons at micro and nanoscale have generated important innovations in the energy storage field [5]. Because of the cost-effectiveness [6,7], the sustainability of the production and the surface properties, activated carbons are one of the main studied materials for electrochemical double-layer supercapacitors [7–9].

The electric double-layer (EDL) development directly depends on the surface area of the carbon material. However, the optimal pore size required is controversial. Some authors defend the importance of micropores contribution in the EDL formation [10], and others highlight the ion diffusional problem of the electrolyte in the narrow micropores and, thus, the better behavior of mesopores [11]. On the other hand, the surface functional groups of carbonaceous material play a key role on the pseudocapacitive reactions on electrodes surface, what improves their capacitances [12–14]. Activated carbons offer the possibility of easy modifying and controlling the porous texture by varying the preparation condition. Besides, they can be submitted to thermal and chemical processes to enlarge the porosity or enhance the surface chemistry. Chemical activation with H_3PO_4 allows for obtaining activated carbon with a high development of the porosity [15], generating narrow mesoporous [16]. This should avoid the ion diffusional problem in the thinner micropores, enhancing the carbon capacitor performance [17].

The influence of heteroatoms like P or N on the electrochemical activity of the carbonaceous material, as well as the pseudocapacitive redox reaction of surface groups containing these atoms has been widely studied [18,19]. In fact, some phosphorus functional groups remain fixed on the carbon surface during the activation process, which is beneficial for the electrochemical carbon behavior [20]. On the other hand, nitrogen surface groups, along with oxygenated groups, are the most investigated heteroatom surface groups in the literature due to: (i) the presence of these atoms in biomass precursors [21,22], (ii) the better electric conductivity due to the conjugation of the nitrogen lone-pair electron and the carbon π-system [23,24], and (iii) the

electrochemical synergy of N-chained groups with oxygenated or P-surface groups [13,18]. Apart from this N-P synergy, it has been proved that P-groups remaining after chemical activation with phosphoric acid play a key role on the nitrogen functionalization of the carbon surface [25]. This strategy allows for obtaining N-enriched activated carbons from a N-free lignocellullosic raw material, what considerably opens the possibilities of producing functionalized activated carbons.

Different nitrogen oxidation states and forms have been reported and the importance of some of them (pyridinic nitrogen, quaternary nitrogen…) on the pseudocapacitance of an activated carbon electrode has been described [26–28]. Although the positive influence of nitrogen on carbon electrodes are extendedly accepted, nitrogen-enriched carbons usually present more than one structure of nitrogen, hindering the possibility of studying the contribution of each one or the inert character of some of them [13,23,26–29]. In this line, our research group has developed different methods for selectively obtaining each of the most common surface nitrogen groups studied (almost isolated) by chemical or thermal treatments of a phosphorus-containing activated carbon [25,30]. In this work, different nitrogen surface functionalities have been selectively prepared on a phosphorus-containing activated carbon and their electrochemical performances have been studied in order to elucidate the electrochemical contribution of each nitrogen surface group.

2. Experimental

2.1. Activated carbon preparation

Olive stone (OS), as lignicellulosic raw material, was chemically activated to obtain phosphorus-containing activated carbons [31]. The precursor was impregnated with H_3PO_4 85 wt%, with an impregnation ratio (wt. H_3PO_4/wt. OS) of 3, and was dried at 60 ºC for 24 h in a vacuum dryer. Then, the substrate was submitted to a carbonization treatment at 500 ºC under a continuous N_2 flow (150 cm^3 min^{-1}), the final temperature was maintained for 2 h. The activated carbon was then washed with distillated water at 60 ºC to remove H_3PO_4. The obtained activated carbon, named ACP, presented a yield of 44.8 wt%.

2.2. Activated carbon functionalization

ACP was functionalized by a nitric acid treatment [25]. ACP was contacted with a 5 M HNO_3 solution (1 g of ACP in 50 cm^3) with a continuous stirring at 80 ºC for 3 h. The surface-oxidized activated carbon was washed until constant pH in the eluate and was used as the nitrogen-enriched activated carbon precursor for obtaining the rest of the functional groups. The nomenclature used for this sample was ACP-N [25].

ACP-N was submitted to different chemical and thermal reduction processes to modify the nitrogen oxidation state [30]. Chemical reduction was carried out by mixing 50 cm^3 of an ACP-N solution in ethanol with 50 cm^3 of a $NaBH_4$ (reducing agent) solution in ethanol. $NaBH_4$ solution was slowly dripped over the carbon solution, and was maintained for 24 h with continuous stirring. The final activated carbon was washed with distillated water at 60 ºC. Activated carbons yielded by this method were named by adding –B to the nomenclature (i.e. ACP-NB). On the other hand, a mild and a severe thermal reduction of the nitrogen-functionalized activated carbon were carried out by thermal treatments under inert atmosphere at 300 and 930 ºC, respectively. Activated carbons obtained were named by adding –Δ and –HT, for the mild and severe thermal reduction process, respectively. A detailed description of the reduction treatments can be found elsewhere [30].

Amido-amino groups were incorporated to the carbon through a sequential treatment for acyl chloride formation and amidation reaction. Firstly, ACP-N was contacted with thionyl chloride (1 g of ACP-N in 37.5 cm^3) under continuous stirring, at 70 ºC for 5 h, in order to transform carboxyl groups into acyl chlorides ones. Once washed with isopropyl alcohol and oven-dried, this intermediate activated carbon was treated with ethylendiamine, under continuous stirring at 90 ºC for 24 h. The corresponding (amido-amine)-containing activated carbon (ACP-E) was yielded after washing with methanol, and then with distilled water until constant pH.

Propagation of poly(amido-amine) dendrimers (PAMAM) on ACP-E was performed by sequential alkylation and amidation treatments. Firstly, Michael addition was carried out in a stirred tank at 50 ºC for 24 h. Methyl acrylate and methanol were mixed in 1:4 (cm^3:cm^3) ratio with ACP-E. Subsequently, amidation was carried out under the same conditions mixing the resulting activated carbon with ethylendiamine and methanol with a ratio of 1:2 (cm^3:cm^3) to obtain the first (ACP-E1) poly(amido-amine) generation. The second (ACP-E2) generation of poly(amido-amine)-fuctionalized

activated carbon was prepared from ACP-E1 by using a double proportion of methyl acrylate (ratio 1:2) in the Michael addition reaction and of ethylendiamine (ratio 1:1) in the amidation reaction.

2.2. Activated carbon characterization

The porous texture of the activated carbons was characterized by N_2 adsorption-desorption at -196 ºC and CO_2 adsorption at 0 ºC, using a Micromeritics ASAP2020 apparatus. Samples were previously outgassed for 8 h at 150ºC under vacuum. The apparent surface area (A_{BET}) was calculated using the BET equation from the N_2 adsorption-desorption isotherm. Micropore volumes were estimated with the Dubinin-Radushkevich equation from N_2 adsorption-desorption isotherms and CO_2 adsorption isotherms, obtaining information about the adsorption in the range of micropores (V_{DR}^{N2}) and narrow micropores (V_{DR}^{CO2}), respectively.

The surface chemistry was analyzed by X-ray photoelectron spectroscopy (XPS) analysis and by temperature-programmed desorption (TPD) experiments. XPS analyses were carried out in a 5700 C model Physical Electronics apparatus with MgKα radiation (1253.6 eV). The C1s peak position was set at 284.5 eV [16] and used as reference to locate the other peaks. TPD experiments were carried out in a customized quartz fixed-bed reactor placed inside an electrical furnace. CO and CO_2, as output gases, were measured by a non-dispersive infrared (NDIR) gas analyzer, Siemens ULTRAMAT 22. 80 mg of the carbon sample was heated from room temperature to 930ºC at a heating rate of 10 ºC min^{-1} under N_2 flow (200 cm^3 min^{-1}).

Ninhydrin test was carried out in order to analyze the presence of primary amino groups fixed in the activated carbon surface. A 10 mg cm^{-3} solution of Ninhydrin in ethanol (96%) was added to the activated carbon in a stirred tank microreactor at 85 ºC for 45 min. At these conditions, ninhydrin reacts with the primary amino groups forming a condensed molecule from ninhydrin, ammonia and the intermediate hydrindatin, and yielding a blue-colored solution. Detailed information of this test, we have adapted from the classical ninhydrin method [32], can be found elsewhere [30].

Activated carbon particles morphology was studied by scanning electron microscopy (SEM), using a JSM 6490LV JEOL microscope working at 25 kV. Particle size distributions were estimated with an image analyzer software. The C, O, P and N atomic

distribution of the particle surface was analyzed in a FEI Quanta 250 FEG Scanning Electron Microscope equipped with energy-dispersive X-ray analyses (SEM-EDX).

The electrochemical performance was investigated in a standard three electrode cell using a platinum wire as counter electrode and Ag/AgCl electrode as reference electrode. Activated carbons were ground (to powder) and dried at 100 ºC before the preparation of the working electrode. The working electrode, 10 mg of a slurry of 80% activated carbon, 10% acetylene black as conductivity promoter and 10% polytetrafluoroethylene (PTFE) as binder, was dried at 100ºC in a vacuum oven and then pressed into a stainless steel mesh (used as current collector) at 2 tons during 5 min to ensure a homogeneous and comparable electrode thickness (c.a. 250 μm). Working and counter electrodes were placed face-to-face and tested in 1 M H_2SO_4 solution as electrolyte. Samples were characterized by cyclic voltammetry technique at different scan rates (0.25 and 1 mV s^{-1}) in an electrochemical analyzer, model 600D Series (CH Instrument Inc.). The specific capacitances (C_g) of samples were calculated from the area of the voltammogram as follows:

$$C_g = \frac{\int j \, dE}{\nu \, \Delta E} \quad (1)$$

where the numerator represents the voltammogram area, ν is the scan rate and ΔE is the working potential window (0.8 in all cases). The above calculations were performed with the third voltammetric cycle with a stable plot in order to avoid the physisorbed oxygen influence. Specific capacitances are related to the mass of active material (F g^{-1}), and surface capacitances to the specific surface area (mF m^{-2}).

3. Results and Discussion

Fig. 1 summarizes the preparation routes of the different activated carbons, and the details of the nomenclature of each carbon type. As can be observed, five different treatments were used in order to synthesize the nitrogen-enriched activated carbons: (i) an oxidation/nitration of the initial activated carbon, (ii) a chemical reduction with $NaBH_4$, (iii) a thermal reduction at low temperature, (iv) a thermal reduction at high temperature and (v) a chemical treatment with ethylendiamine/methyl acrilate to produce PAMAM on the carbon surface.

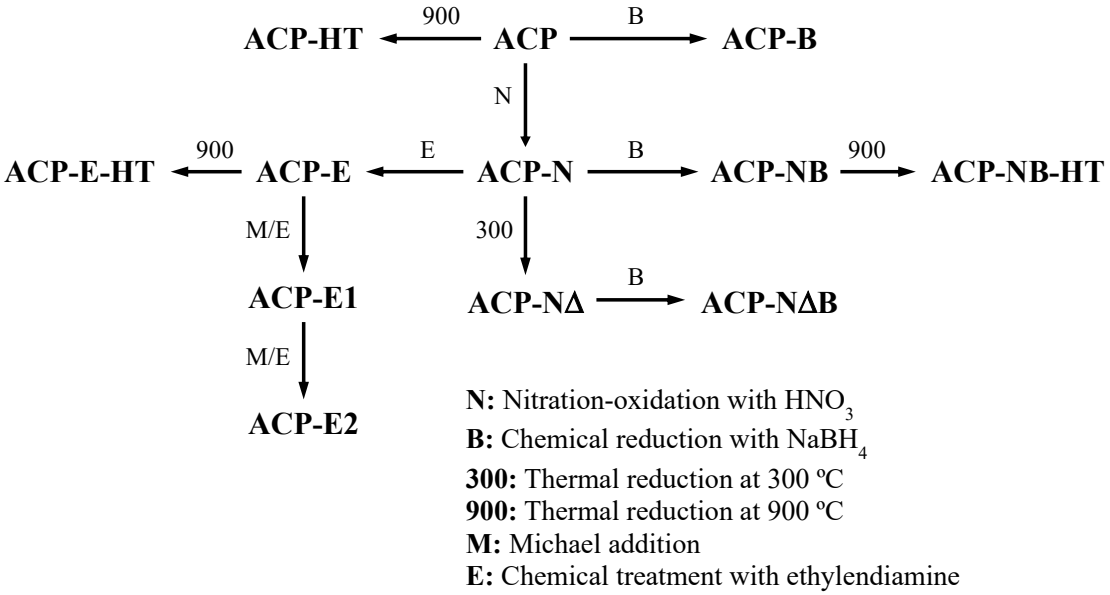

Fig. 1. Chemical and thermal routes for obtaining the functionalized activated carbons.

Fig. 2 shows the N1s spectrum obtained from XPS analyses of the main activated carbon prepared: ACP-N, ACP-NB, ACP-NΔ, ACP-E and ACP-NB-HT. Five contributions of different nitrogen functionalities can be located at 405.5, 401.2, 400.4, 399.4 and 398.9 eV initially attributed to nitro ($-NO_2$), quaternary nitrogen (N-Q), pyrrolic (N-5) amino ($-NH_2$) and pyridinic (N-6) groups, respectively [33]. ACP-N presents an unique peak at 405.5 eV associated to nitro groups [25]. Chemical reduction with $NaBH_4$ yields a N1s spectrum with an only peak centered at 399.4 eV, related to the presence of amino groups on its surface (ACP-NB)[30]. A similar result is obtained with ACP-E. This sample exhibits a peak, slightly shifted to higher binding energies, which could be associated to the presence of $-NH_2$ and -NHR groups (from the amido-amino functional groups). On the other hand, N1s spectrum of thermally reduced carbon at 300 ºC (ACP-NΔ) shows two differentiated peaks, the first one can be associated to the presence of two different species, located at 400.4 and 398.9 eV, and corresponding to N-5 and N-6 structure, respectively; the second one corresponds to nitro groups (405.5 eV). This result suggests that the mild thermal treatment leads to the partial condensation of the nitrogen structures. N1s spectrum of ACP-NB-HT presents the peaks attributed to the condensed structures N-Q, N-5 and N-6 due to the high thermal stability of these structures. It should be noted that N1s spectra for all activated carbon treated at 930 ºC are quite similar to that illustrated in Figure 1 for ACP-NB-HT.

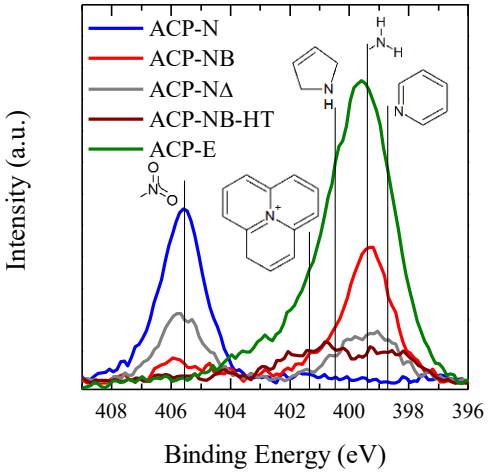

Fig. 2. N1s spectra for ACP-N, ACP-NB, ACP-NΔ, ACP-E and ACP-NB-HT, the different N functional groups are included.

All the nitrogen functional groups incorporated on the carbon surface, along with the ones of oxygen and phosphorus are schematized in **Fig. 3**, where the main groups have been represented. **Fig. 3a** displays the resulting primary and condensed surface groups of nitrogen obtained after the oxidation treatment with nitric acid and the chemical and thermal reductions. As it is well-known, ACP presents different P groups fixed on the carbon, we have illustrated in the scheme one oxidized group (I) and a reduced one (II), more information about the phosphorus surface groups are detailed in previous works [16,34,35]. ACP-N exhibits -NO_2 groups (III) bonded to the ACP structure, whereas the chemical treatment reduces all nitro groups to –NH_2 groups (IV). ACP-NΔ and ACP-NΔB present N-6 and N-5 groups (V and VI, respectively) on their surface, with a nitrogen atom replacing a carbon from 6 or 5 atoms rings. These condensed species, along with N-Q (VII), are identified in all the activated carbons submitted to a severe thermal reduction at 930 ºC. N-Q species are placed inside the polyaromatic structure and are bonded to three carbon atoms, showing a positively charged nitrogen atom. **Fig. 3b** shows the different ramifications of the poly(amido-amine) groups and allows for appreciating the size of each polymeric chain, which causes the aforementioned pore blockage. In this sense, ACP-E shows the shorter amido-amine structures (VIII), and by successive two steps, consisting of Michael addition and amidation with ethylendiamene, it is possible to obtain, as in this case, 1st and 2nd generations of PAMAM chains (IX and X respectively).

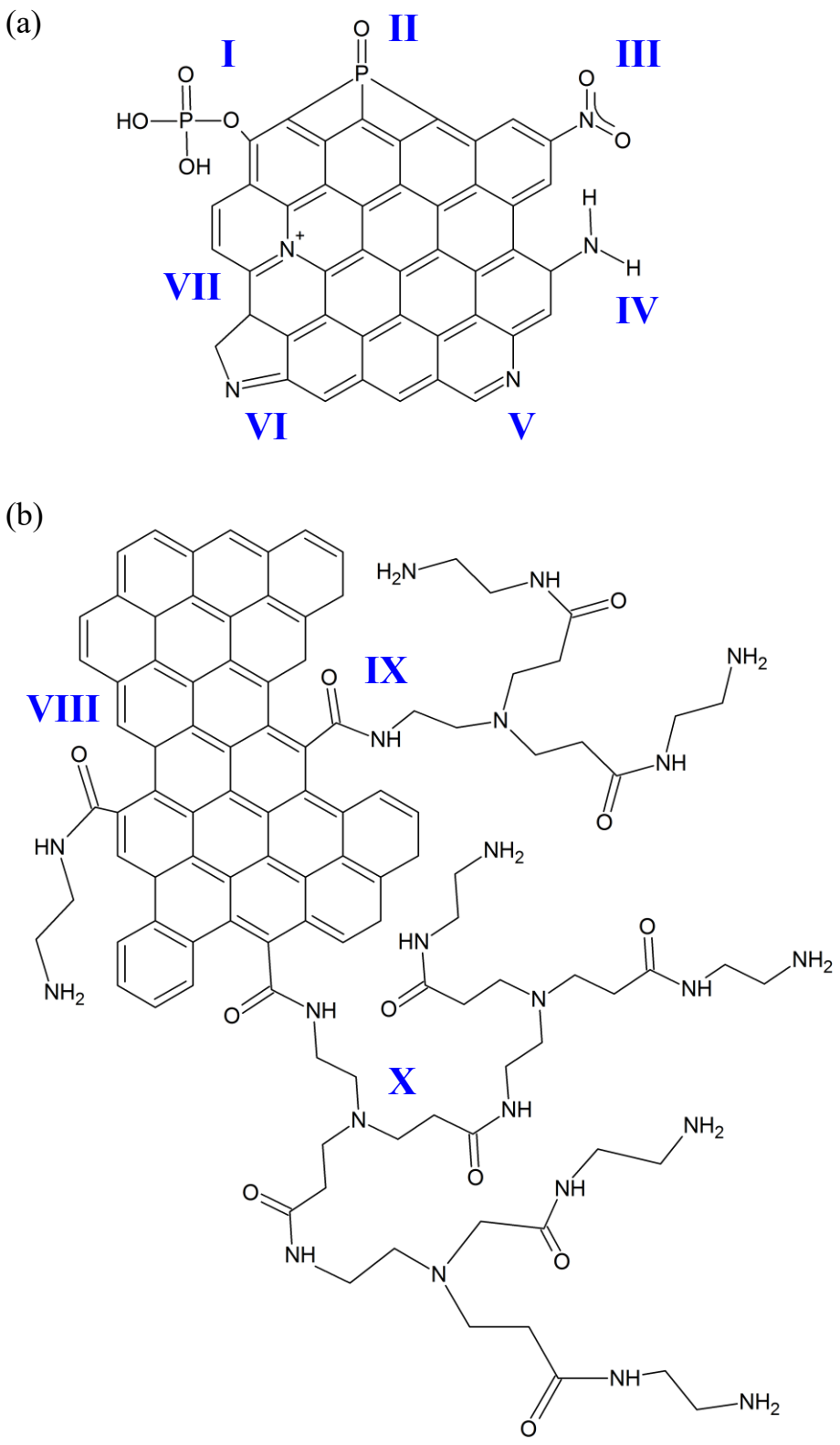

Fig. 3. Schematic illustration of the different surface groups of N-enriched P-containing activated carbons. (a) Primary, condensed and (b) polymeric structures.

Table 1 summarizes the main physico-chemical properties of the parent activated carbon and after the different chemical and thermal treatments. The parameters used for characterizing the porous texture were the apparent surface area (A_{BET}), the micropore volume (V_{DR}^{N2}) and the narrow micropore volume (V_{DR}^{CO2}). As observed, most activated carbons (except for ACP-E1 and ACP-E2) show higher V_{DR}^{N2} values than V_{DR}^{CO2}, which suggests that these materials predominantly present wide micropores (>0.7 nm).

ACP presents a very well-developed porous structure, with an A_{BET} of 1253 $m^2\ g^{-1}$ and a V_{DR}^{N2} of 0.44 $cm^3\ g^{-1}$. However, the decrease of both when activated carbon is submitted to chemical or thermal treatments is significant. Chemical treatment with nitric acid reduces A_{BET} to 984 $m^2\ g^{-1}$ [25], and the chemical reduction treatment with $NaBH_4$ leads to a further reduction of the porosity, showing a decrease of the A_{BET} values of ca. 300 $m^2\ g^{-1}$ between ACP-N and ACP-NB, or ca. 200 $m^2\ g^{-1}$ between ACP-NΔ and ACP-NΔB. The V_{DR}^{N2} also presents a decrease of ca. 0.10 $cm^3\ g^{-1}$ for these activated carbons. The V_{DR}^{CO2} is also reduced from 0.22 (ACP-N) to 0.18 (ACP-NB) and from 0.21 (ACP-NΔ) to 0.16 $cm^3\ g^{-1}$ (ACP-NΔB), respectively [30], this surface deterioration could be associated to the fixation of boron groups (which cause pore blockage) or to the damage of the carbonaceous structure during the chemical reduction.

Table 1. Apparent surface area (A_{BET}) and micropore volume (V_{DR}^{N2}) calculated from N_2 adsorption-desorption isotherm, narrow micropore volume (V_{DR}^{CO2}) from CO_2 adsorption isotherm, atomic surface concentration (%) from XPS analyses and CO and CO_2 evolved amounts from TPD experiments.

Activated carbon	Textural parameters			XPS				TPD	
	A_{BET} ($m^2\ g^{-1}$)	V_{DR}^{N2} ($cm^3\ g^{-1}$)	V_{DR}^{CO2} ($cm^3\ g^{-1}$)	O1s (%)	N1s (%)	P2p (%)	B1s (%)	CO (mg g^{-1})	CO_2 (mg g^{-1})
ACP	1253	0.44	0.19	5.4	0.3	0.9	0.0	56.0	4.4
ACP-B	1004	0.33	0.15	7.1	0.3	0.5	2.3	83.6	12.7
ACP-N	984	0.34	0.22	17.0	2.5	0.4	0.0	134.9	123.6
ACP-NB	682	0.24	0.18	12.5	2.4	0.3	0.7	87.7	62.4
ACP-NΔ	970	0.33	0.21	12.7	1.9	0.3	0.0	167.1	82.7
ACP-NΔB	761	0.25	0.16	12.5	1.8	0.2	0.7	76.5	26.2
ACP-E	550	0.19	0.15	13.2	7.7	1.2	0.0	58.9	36.6
ACP-E1	43	0.01	0.05	11.7	12.4	1.0	0.0	66.1	18.2
ACP-E2	55	0.02	0.05	12.2	11.5	0.9	0.0	93.1	21.8
ACP-HT	1054	0.37	0.21	3.9	0.2	0.8	0.0	n.d.	n.d.

ACP-NB-HT	662	0.23	0.19	6.1	1.4	1.0	1.9	n.d.	n.d.
ACP-E-HT	753	0.28	0.21	4.0	3.2	0.7	0.0	n.d.	n.d.

On the other hand, it is noteworthy that much more accused A_{BET} drop is observed after the PAMAM dendrimers formation (43 m^2 g^{-1}). The preparation method proposed for these nitrogen-rich carbons, a polymerization via alkylation-amidation, allows for obtaining different polymeric brands outside the carbon support. In fact, the reduction of the apparent surface area, from 1253 m^2 g^{-1} (for ACP) to 55 m^2 g^{-1} (ACP-E2), indicates that the polymeric reaction occurs blocking almost totally the carbon pores (V_{DR}^{CO2} of ACP-E2 = 0.05 cm^3 g^{-1}). This result is consistent with the size of PAMAM chains observed in **Fig. 3**.

No significant modifications are observed in the carbon porous texture after a mild thermal treatment. Nevertheless, a decrease of the surface area can be observed after a severe thermal treatment to ACP (ACP-HT) [16,34]. The same thermal treatment carried out to ACP-E showed an opposite trend, A_{BET} value was considerable increased. This result is a consequence of the thermal decomposition of the amido-amino groups (releasing the pore blockage), which has major influence on the porous texture than the collapse of the porosity associated to the high temperature. V_{DR}^{CO2} do not show important changes, suggesting that main modifications of pore structure occur in the range of wider micropores (V_{DR}^{N2} is lower for the N-containing samples) and mesopores.

The nitration-oxidation process of the carbon surface with nitric acid causes an important increase of the oxygen and nitrogen surface atomic concentration (17.0 and 2.5 %, respectively), determined by XPS analyses (**Table 1**). A reduction of the oxygen surface atomic concentration was observed after the chemical reduction treatments (ACP-NB, 12.5 %). However, nitrogen one remains practically constant (2.4 %). A similar trend is observed for the mild thermal reduction treatment in the oxygen concentration, but in this case, nitrogen concentration undergoes a pronounced decrease (1.9 %) due to the decomposition of some NO_2 groups. An important increase of the nitrogen concentration is also observed after the ethylendiamine treatment. The first amido-amine formation on the carbon surface increases by 3 times the nitrogen concentration of ACP-N precursor (ACP-E, 7.7 %), reaching even a major value after

the generation of dendrimer groups (ACP-E1, 12.4 % and ACP-E2, 11.5 %). Both, oxygen and nitrogen concentrations exhibit an important drop after the severe thermal treatment up to 930 ºC, because of the volatile mass loss of the carbon and the reorganization of the carbonaceous structure [33]. Phosphorus surface groups keep fixed to the carbon surface during the different treatments of the activated carbon in relatively lower contents. In this sense, a decrease of the P surface atomic concentration is observed after both chemical treatments with HNO_3 or $NaBH_4$, however, higher concentrations are registered after the treatment with ethylendiamine in the carbonaceous surface. XPS analyses also reveal the presence of boron fixed groups on the surface of the activated carbon treated with $NaBH_4$. The highest boron surface concentration is registered for ACP-B, suggesting that the decrease of phosphorus on nitrogen-doped carbons (ACP-N and ACP-NΔ) can possibly reduce in a great extent the incorporation of boron groups. However, these groups remain stably bonded to the carbon structure after the severe thermal treatment (ACP-NB-HT).

In order to support the results provided by XPS analyses, ninhydrin tests and SEM-EDX analyses were performed. First column of **Fig. 4** shows the results of these ninhydrin tests. This analysis is able to detect selectively amino groups in peptides [32,36], in a previous work we have adapted this test to determine amino groups in carbon samples [30]. The samples treated with $NaBH_4$ and the series of ACP-E carbons were the only samples with positive result in the test (solution in blue). This evidences the presence of amino groups on the surface of these two carbons, in concordance to the XPS results. Therefore, the chemical reduction with $NaBH_4$ provides selectively amino from nitro groups in phosphorus containing activated carbons [30]. However, amino groups are not thermally stable and they probably tend to form condensed structures after the heat treatment up to 930 ºC (ACP-NB-HT, **Fig. 2**). **Fig. 4** also displays the presence of C, O, P and N atoms in activated carbon particles obtained from SEM-EDX analyses. As observed, both P (fixed in the chemical activation process) and N (fixed in the subsequent functionalization treatments) show uniform distribution all over the activated carbon particles, which suggests that the functionalization with nitric acid leads to a dispersed nitrogen in the activated carbon. These results are also consistent with those previously reported [25], where we proposed that nitrogen groups are anchored during the functionalization treatment near to the phosphorus sites of ACP.

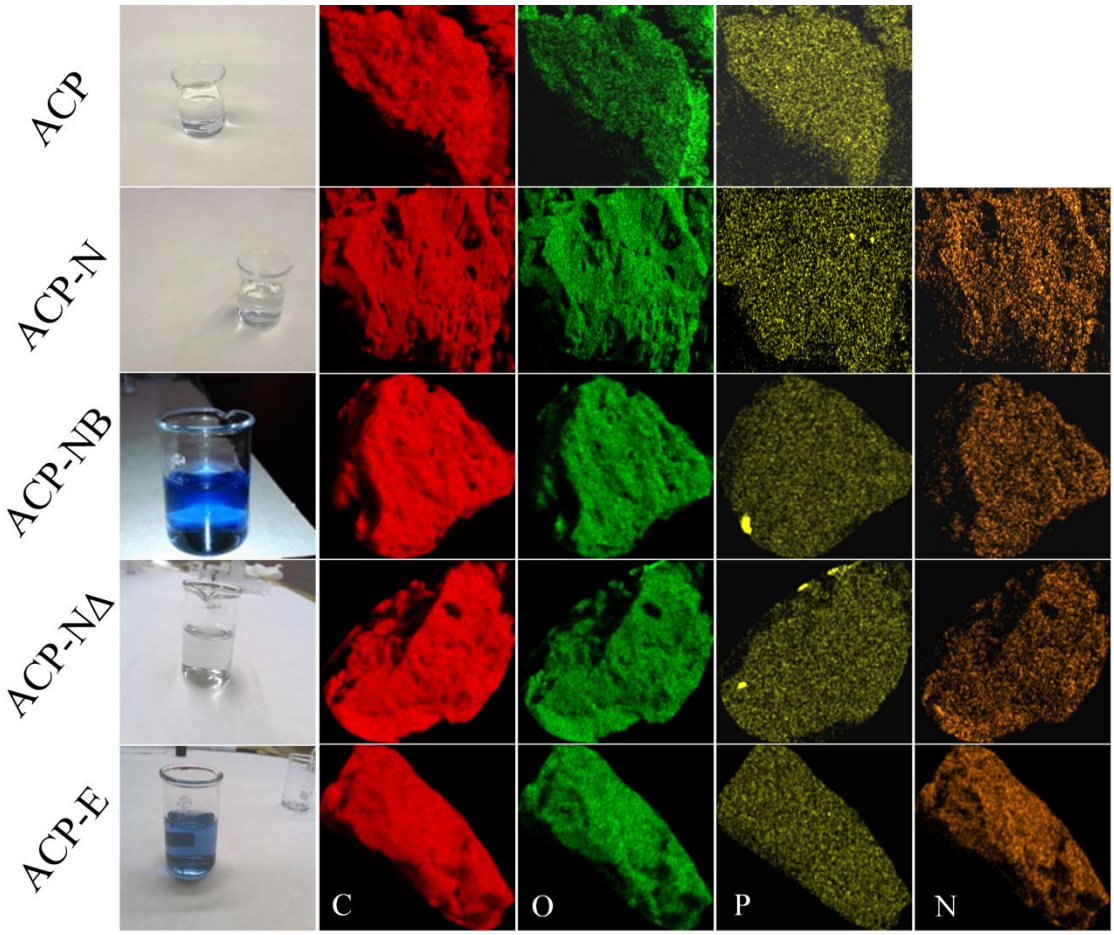

Fig. 4. Ninhydrin test and atomic dispersion mapping from SEM-EDX of ACP, ACP-N, ACP-NB, ACP-NΔ and ACP-E

Regarding the CO and CO_2 evolved amounts shown in **Table 1**, the functionalization process with nitric acid increases the surface carboxylic acid groups concentration, consequently, it can be observed an increase in CO_2 evolution (from 4.40 for ACP to 123.57 mg g^{-1} for ACP-N). According to the low thermal stability of CO_2-evolving groups [37], and the high thermal resistance of C-O-P groups, which evolves a CO [16,38], the series of activated carbons submitted to a mild thermal treatment (ACP-NΔ and ACP-NΔB) presents a lower CO_2 evolved amount than their precursor (ACP-N and ACP-NB). ACP-E, ACP-E1 and ACP-E2 exhibit similar amounts of evolved CO and CO_2 than the other functionalized activated carbons, but it can be observed in case of PAMAM functionalization (ACP-E, ACP-E1 and ACP-E2) that the CO evolution increases as the amide groups, meanwhile the CO_2 evolved remains practically the same. TPD analyses also reveal that most samples studied mainly contain oxygenated surface groups evolving as CO. According to the literature, these oxygenated groups are

more electrochemically active than CO_2-evolving groups because of the possible presence of quinone/phenolic groups [39–41].

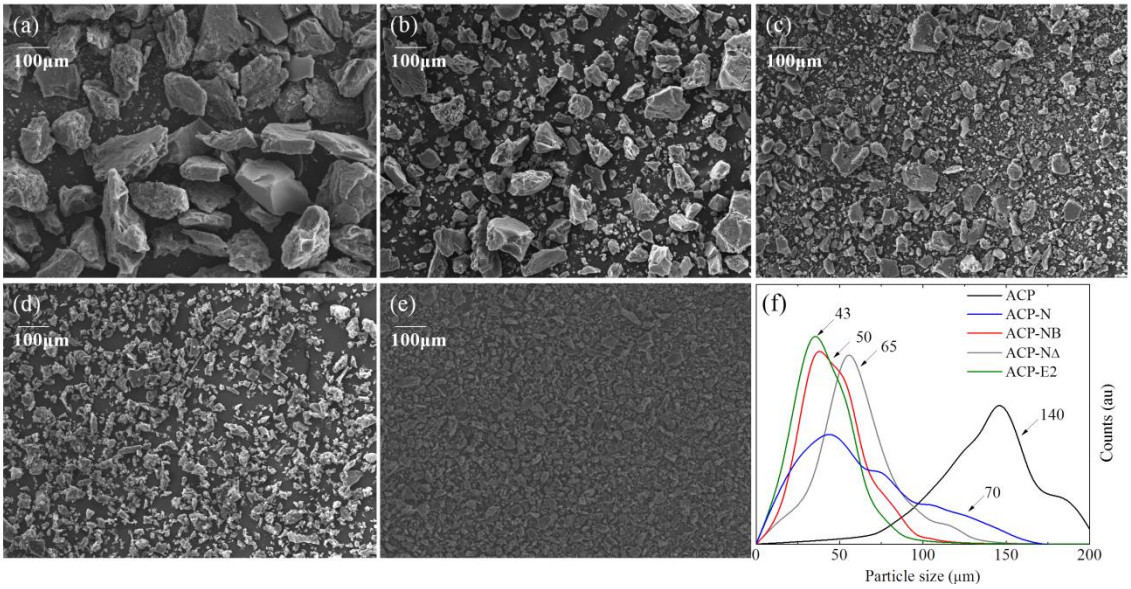

Fig. 5. SEM micrographs of (a) ACP, (b) ACP-N, (c) ACP-NB, (d) ACP-NΔ and (e) ACP-E2 and (f) particle size distribution of these activated carbons.

Fig. 5a-e displays SEM micrographs for the different activated carbons. ACP (**Fig. 5a**) presents grains with similar shape and uniform particle sizes. In general, it can be observed a reduction of the particle sizes after the different treatments due to the erosion of the particle in the stirring process and/or the chemical abrasion of the particle surface. ACP-N and ACP-NB (**Figs. 5b** and **5c**, respectively) display a large range of different particle sizes, which evidences the important destruction of some grains, overall in the sample treated with $NaBH_4$. Samples ACP-NΔ and ACP-E2 (**Fig. 5d** and **5e**, respectively) show much lower and uniform particle sizes, suggesting the harsh erosion of the carbon particles after a series of successive treatments.

Fig. 5f depicts the particle size distribution of these activated carbons obtained with an image analyzer software from five images of each sample similar to those in **Fig. 5a-e**. As it is possible to observe, ACP presents clearly higher particle sizes with an average particle size of 140 µm. ACP-N shows a broad particle size distribution, with a mean diameter of 70 µm. This last activated carbon undergoes an additional reduction of the particle size with the thermal (ACP-NΔ) and chemical (ACP-NB) reduction treatments, obtaining more uniform particles sizes distributions with mean values of 65 and 50 µm,

respectively. ACP-E2, which was submitted to the most severe treatments, shows a narrower particle size distribution, close to an important reduction of the particle size (mean diameter = 43 μm).

The abovementioned activated carbons were tested in a three electrode cell with 1M H_2SO_4 solution as electrolyte to evaluate the role of the different nitrogen surface groups. Cyclic voltammetries were carried out at a scan rate of 1 mV/s. **Fig. 6** shows the cyclic voltammograms of ACP and the different nitrogen-enriched carbons prepared from it. As can be seen, ACP exhibits a quasirectangular cyclic voltammogram (CV), typical of an essentially capacitive process associated with the formation of the electric double layer (EDL), with the presence of only a little hump associated to redox reactions of the oxygen and phosphorus surface groups (5.4 and 0.9 % surface atomic concentrations, respectively) [20]. The high porosity of ACP enhances the ion diffusion into the carbon pores and the development of the EDL [42].

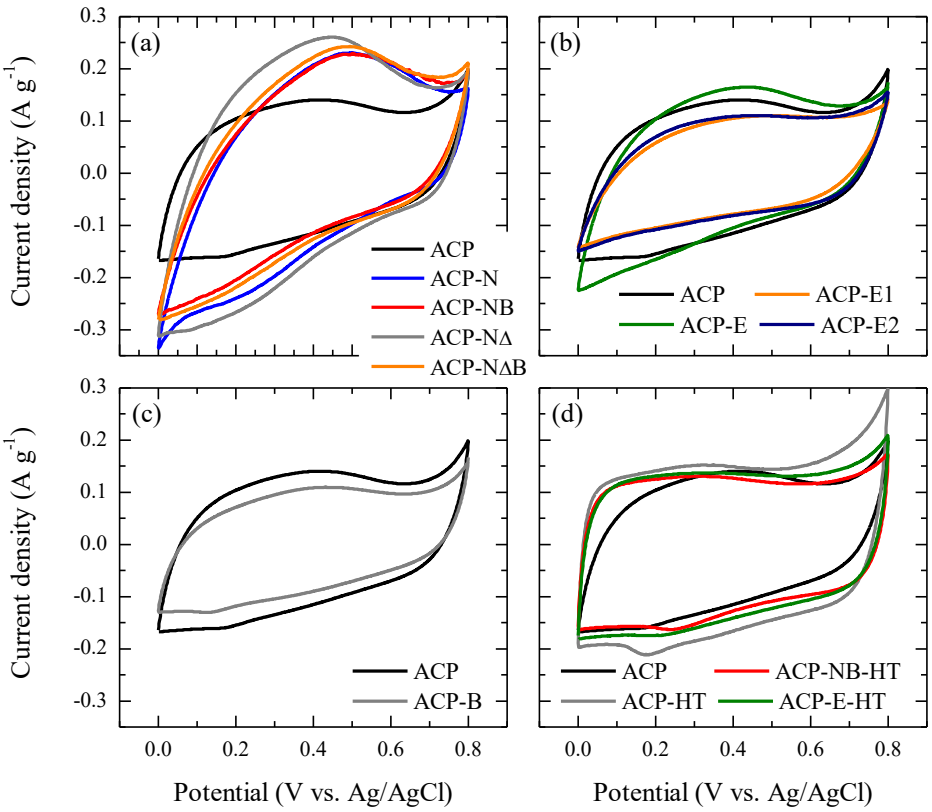

Fig. 6. Cyclic Voltammograms of (a) Nitro/Amino-containing ACP, (b) Amido-amine-containing ACP, (c) boron-containing ACP and (d) Quaternary Nitrogen-containing ACP in H_2SO_4 1 M. Scan rate: 1 mV s^{-1}

370

Fig. 6a also displays the CVs of functionalized activated carbon with -NO_2, -NH_2, N-5 and N-6 surface groups. This series of activated carbons (named ACP-Ns) shows different CV shapes, and seems to present more defined peaks due to redox reactions on the carbon surface groups, instead of the rectangular voltammogram due to the EDL. **Fig. 6b** shows the CVs of the ACP-E carbon series (ACP-Es, activated carbons containing amido-amine and poly(amido-amine) surface groups). The shape of the voltammograms is quite similar to that of ACP, and different to those of the ACP-Ns series. In this sense, **Table 1** displays a nitrogen contents in ACP-Es series five times higher than those observed in ACP-Ns one. Therefore, the type of nitrogen group plays an important role in the pseudocapacitance reactions of those activated carbons.

As aforementioned, boron was fixed on the carbon surface, during the chemical reduction process, with sodium borohydride. A blank test was carried out by treating ACP with $NaBH_4$ in order to evaluate the possible electrochemical performance of deposited boron. **Fig. 6c** shows the corresponding ACP-B voltammogram, which is similar to that obtained for ACP, however, the internal area of the voltammogram decreases for ACP-B. This could be related to the decrease of the specific surface area of the ACP-B, as can be observed in **Table 1**. These results suggest that boron surface groups cause a pore blockage on ACP limiting the ion diffusion, and thus, ACP-B develops a smaller EDL.

Fig. 6d shows the CVs of all the high temperature heat-treated (ACP-HTs) carbon series. ACP-HTs develop a well-defined EDL, with a perfect box-like voltammogram without any accused peaks between 0 and 0.7 V (vs. Ag/AgCl reference electrode). Comparing with the more distorted voltammogram exhibited by ACP-Ns (**Fig. 6a**), these electrodes show lower internal resistance, which suggest an improvement of the conductivity of the electrodes upon increasing the carbonization temperature. This carbon series only shows a little hump at 0.2 V (in the reduction brand), which could be attributed to the P-groups in ACP-HT [40]. All of the carbons of this series present a

very similar voltammogram shape. Compared to ACP electrode, the area of the voltammograms of ACP-HTs are higher, which can be explained by the formation of more ordered carbon structures, the presence of ultra-stable C-P surface groups, the minimum modification of the microporosity, and the presence of N-Q (N^+, electron deficient) groups, which can favor the electronic conductivity of the electrode [23,43,44]. It could be observed that no matter from which the quaternary nitrogen-rich activated carbons are obtained, the electrochemical behavior is similar. In this way, the redox reaction, that causes a peak appearance at ca. 0.4 V in ACP-Ns CV, is not observed when the activated carbons are submitted to the heat treatment, which produces disappearance of nitro/amino groups in favor of mainly N-Q groups (with some N-5 and N-6).

In this context, **Fig. 6** represents three clearly differentiated behaviors. Firstly, a group of nitrogen-functionalized carbons that shows redox surface reactions. This enlarges the CV area due to a pseudocapacitance contribution (ACP-Ns). Secondly, PAMAM functionalized carbons (ACP-Es), which exhibit very low BET specific surface areas. The CV of these three carbons materials present a surprisingly big area and rectangular shape, in spite of the low surface area (A_{BET}). Lastly, a group of activated carbons, treated at high temperatures with C-P-O and N-Q surface groups (apparently with higher conductivity), which shows a very fast development of the EDL.

Specific capacitance (C_g) is a normalized quantitative measure of the CV area and is function of different variables such as A_{BET}, CO-type oxygenated surface groups content (mainly quinone-phenolic groups) [40], and/or the amount of electrochemically active heteroatoms (as nitrogen) [13,23]. **Table 2** shows the C_g and the surface capacitances calculated from the voltammogram area of all the activated carbon electrodes. As can be seen, ACP exhibits a C_g of 204 F g^{-1}. After the treatment with $NaBH_4$ (ACP-B) the specific capacitance is reduced to 157 F g^{-1}. However, the surface capacitances of both activated carbons are very similar (163 and 156 mF m^{-2}, respectively), suggesting that boron groups only causes the pore blockage, hindering the EDL development.

Table 2. Specific and surface capacitances of all the samples in H_2SO_4 1 M, at a scan rate of 1mV s^{-1}.

Electrode from	C_g (F g^{-1})	C_g/A_{BET} (mF m^{-2})
ACP	204	163
ACP-B	157	156
ACP-N	256	260
ACP-NB	241	353
ACP-NΔ	317	327
ACP-NΔB	266	350
ACP-E	209	380
ACP-E1	140	3256
ACP-E2	152	2764
ACP-HT	296	281
ACP-NB-HT	236	357
ACP-E-HT	256	340

On the other hand, an increase of both specific and surface capacitances respect to the initial ACP electrode was observed in ACP-N. It could be seen that this oxidation treatment does not only cause a drop of A_{BET}, but also introduces oxygen and nitrogen surface groups (**Table 1**). The reduction of nitro-groups with sodium borohydride practically does not decrease the C_g, however the surface capacitance increases. These results, along with the aforementioned CV shape modification, suggest that redox reactions of these nitrogen surface groups play a key role in this increment of capacitance values. Besides, the introduction of N-5 and N-6 surface groups, which electrochemical activity is extendedly accepted [23,26], improves the C_g values of ACP-NΔ and ACP-NΔB, increasing the surface capacitances to higher values than 300 mF m^{-2}, which are considerably higher than some values reported in the literature for nitrogen doped carbon [14].

Amido-amine and poly(amido-amine) functionalized carbons show singular C_g values in comparison to the other electrodes tested. ACP-E, as poly(amido-amine) precursor, displays similar C_g than that of the initial ACP with practically half of A_{BET}. This tendency remarks the importance of surface groups despite the absence of pseudocapacitive peaks in the CV of these carbon electrodes. Surprising results have

been observed for the two dendrimers generation (ACP-E1 and ACP-E2) with specific surface areas about 55 $m^2 g^{-1}$, C_g of approximately 150 F g^{-1} and surface capacitances arond 3000 mF m^{-2}. These significant surface capacitances values are similar to those previously reported by Hulicova et al. [21,27] for nonporous carbonaceous materials with high nitrogen surface concentration obtained from melamine. In our case, the values of surface capacitance are in the same order of magnitude (3256 mF m^{-2} vs 3660 mF m^{-2}), but our gravimetric capacitances are more than double (140 F g^{-1} vs 62.26 F g^{-1}). Furthermore, our materials present additional environmental advantages, since they are derived from lignocelullosic waste.

High temperature-treated activated carbons (ACP-HTs) present high values of C_g (near to 300 F g^{-1}). ACP-HT exhibits higher C_g than its counterpart (ACP) despite the porous structure partially collapse after the heat treatment. This result suggests that the improvement of the carbon surface properties with the thermal treatment, such as the enhancement of the structural order, has more influence on the C_g than the shrinkage of the porous texture. C_g values obtained for ACP-NB and ACP-NB-HT are very similar, however, the content of N decreases from 2.4 to 1.4 %, suggesting the further contribution of a more ordered structured associated to the high temperature treatment (EDL capacitance may be similar as both carbons present similar A_{BET}). The aforementioned development of the porosity and formation of N-Q groups are evidenced in the C_g values of ACP-E-HT and ACP-E. Regarding the results of surface capacitances, the importance of N-Q presence on the electrochemical behavior of carbons is appreciated, reaching values of 357 and 340 mF m^{-2} (for ACP-NB-HT and ACP-E-HT, respectively), in comparison to 281 mF m^{-2} for ACP-HT.

Cyclic voltammetries were also carried out at very low scan rate. **Fig. 7** depicts the CVs of ACP-Ns and ACP-Es at 0.25 mV s^{-1}. ACP-Ns exhibit a clearly defined peak around 0.35 V (in the oxidation brand) compared to ACP, which makes bigger the CV area because of the pseudocapacity contribution (**Fig. 7a**). Activated carbons with oxygenated surface groups usually present a par redox at 0.4V in acid electrolyte, due to reversible redox reactions associated to quinone/phenol transformations [45]. This redox process is accentuated in carbons with high content of CO-type surface groups and low content of CO_2-type functional groups. According to this premise, ACP should exhibit a pronounced peak due to the high CO/CO_2-type group ratio, however this redox

process is insignificant in ACP. Hence, the peak at 0.35 V observed in ACP-Ns cannot be directly related to quinone/phenol switch. These results support the hypothesis that the presence of nitro and/or amino groups improves the electrode behavior due to the presence of pseudocapacitive processes.

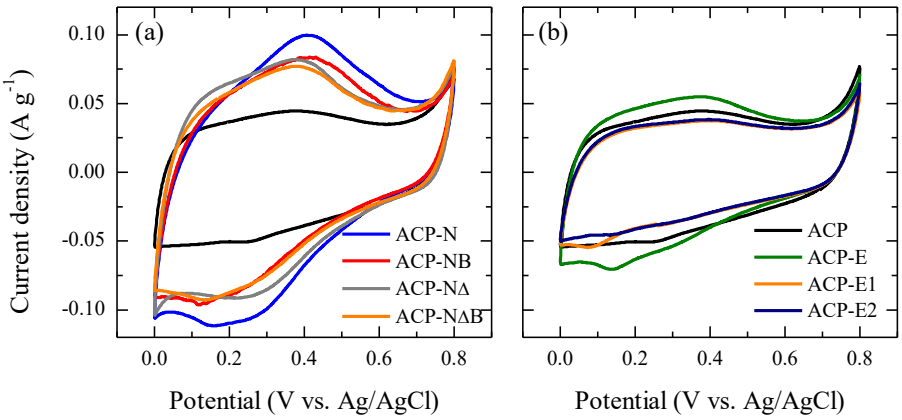

Fig. 7 Cyclic Voltammograms of (a) Nitro/Amine-containing ACP and (b) Amido-amine-functionalized ACP in H_2SO_4 1 M. Scan rate: 0.25 mV s^{-1}

Fig. 7a also shows the ACP-NΔ and ACP-NΔB voltammograms. The CV curves display a distorted box-like shape. ACP-NΔ voltammogram presents a slope variation of the oxidation brand at 0.05 A g^{-1} and a slight displacement of the pseudocapacitive peak to lower potential in the oxidation brand and to higher potential in the reduction one (compared to ACP-N). This displacement implies an improvement in the redox reaction kinetic. These results can be explained by the introduction of N-5 and N-6 groups after the thermal reduction treatment. These condensed nitrogen structures (pyrrolic and pyridinic groups) enhance the electronic and ionic conductivity of the carbon due to the conjugation of the unpaired electrons of the nitrogen atom with the π-system of the aromatic rings [27,46]. Ions can diffuse on the electron surface easily and the electric double layer is faster developed, modifying the CV shape to a more rectangular voltammogram. Likewise, the electron-donor capability of this nitrogen groups [21] could favor the catalytic activity in electron-transfer reactions, making them faster.

Fig. 7b illustrates the CVs of ACP-Es at low scan rate and, as can be seen, both shape and size can be comparable with ACP voltammogram, and do not seem to be as

electrochemically active as ACP-Ns. As occurs at higher scan rate, (amido-amine)-containing activated carbons develop a rectangular CV despite both of them are almost nonporous carbons. Zhang et al. demonstrate that polyethylendiamino groups contribute to the efficiency of electrode by increasing the current density [47]. Similar carbon materials, with very low A_{BET} and high surface nitrogen content, have been already studied as supercapacitors because of the excellent surface capacitance [27,48].

In this case, the rectangular shape of the CV is not related to the formation of the double layer, due to the low A_{BET}. Some authors related the pseudocapacitive behavior to nitrogen and oxygen electrochemical reactions or to the improvement of charge mobility in the carbon surface [27,48]. In both scenarios, it is essential to assure the presence of nitrogen on the external carbon surface, since nitrogen seems to be the main source of this pseudocapacitive behavior.

For the sake of studying the possible participation of nitrogen and phosphorus groups in redox reactions, and their possible chemical changes, ACP-N, ACP-NB and ACP-E were submitted to different electro-reduction/oxidation treatments and they were analyzed by XPS analyses. ACP-N was submitted to a constant reduction potential of -0.2 V (vs. Ag/AgCl reference electrode) for 5 min. At this potential, the activated carbon keeps on showing a rectangular voltammogram and does not appear any cathodic current of hydrogen generation, so this potential corresponds to a mild reduction treatment of the carbon electrode. On the other hand, when ACP-N was submitted to a severe reduction potential (-0.8 V), the electrode reaches the limit of the cathodic current in which carbon structure is no longer stable. **Fig. 8a** displays the N1s spectrum of original ACP-N and the samples submitted to a mild and a severe reduction process. An important variation of the spectrum is observed for electrochemically treated ACP-N. In this sense, the appearance of a new peak at lower binding energy is observed (ca. 402 eV). In addition, the presence of $–NO_2$ groups after the mild reduction process and its absence after the severe one suggest that the more the reduction potential is, the more conversion of $–NO_2$ group is obtained. As can be observed, the new peak of the spectrum appears far from the characteristic amine binding energy. Therefore it is not possible to obtain $–NH_2$ groups from $-NO_2$ by this electrochemical method despite ACP-N was submitted to the maximum reduction potential resisted.

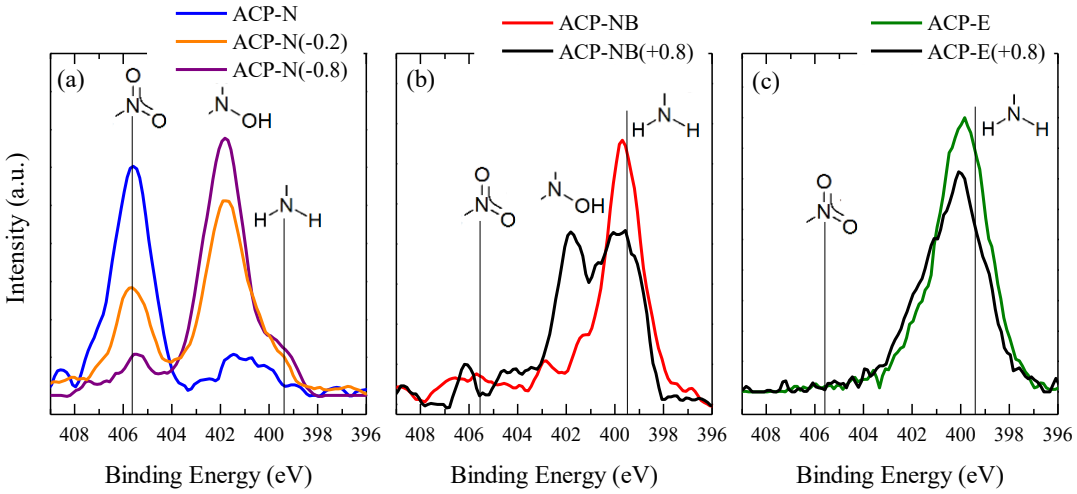

Fig. 8. N1s spectra of (a) ACP-N, (b) ACP-NB and (c) ACP-E electrodes and their resulting electrodes after reduction and oxidation treatments

The opposed test was carried out with ACP-NB and ACP-E. In these cases, both samples exhibit a peak at 399.4 eV in N1s spectrum, associated to -NH_2 group. Activated carbons were submitted to a mild and a severe oxidation process, being the potential used for each treatment 0.8 and 1.1 V (vs. Ag/AgCl reference potential) respectively, and the exposure time 5 min. As occurred before, these potentials correspond to the end of the rectangular voltammogram and to the limit of the carbon electrode stability.

Figs. 8b depicts the N1s spectrum for the resulting ACP-NB activated carbon after the oxidation process and **Fig. 8c** displays the corresponding one to ACP-E electrode. In both, the results for only one oxidation process were represented because of the similarity of the data obtained with the mild and the severe electrochemical treatment. On one hand, ACP-NB undergoes the same changes observed for ACP-N. Thus, a new peak appears centered at ca. 402 eV, but in this case it is not possible to oxidize all –NH_2 surface groups. Likewise, it is not possible to obtain –NO_2 group from amine, and the species obtained correspond to an oxidized species of nitrogen but not the most oxidized one. On the other hand, the N1s spectrum of ACP-E does not present any modification after the electro-oxidation treatments. These results suggest that amido and aliphatic amino groups are resistant to be electro-oxidized and do not change its oxidation state during the electrochemical process. Furthermore, the appearance of a new nitrogen species at ca. 402 eV could be related with the peak of the CV observed in

ACP-N and ACP-NB, inasmuch as ACP-E does not show any modification of the nitrogen surface groups and exhibits a rectangular voltammogram. This peak at 402 eV could be associated to an oxidized nitrogen group (N-X) which presents higher oxidation state than N-5, N-6 or N-Q, but lower than NO_2, as that presented in a simple N-O bond. Many authors usually related N-X compounds to oxidized pyridinic groups because they could be obtained from N-6 groups by forming the N-O bond [23,27,49]. In any case, these N-X compounds, which present a simple N-O bond, must be obtained from nitro and from amino groups bonded to aromatic or basal carbons in ACP, according to the above results. On this basis, the form of this N-compound could be associated to hydroxylamine structures, with a simple N-C bond and one or two hydroxyl groups (hydroxylamine, C-NHOH or dihydroxylamine C-$N(OH)_2$, respectively). In this sense, amino oxidation on carbon electrodes surface is a well-known redox reaction, which is accepted by many authors as the reason of the enhancement of the (pseudo)capacity in N-containing carbon electrodes [27,50,51].

Likewise, P2p spectra were also analyzed after the electrochemical reduction and oxidation treatments in order to elucidate the possible modifications of P oxidation state. XPS spectra of P2p for ACP-N, ACP-NB and ACP-E are depicted in **Fig. 9**. Phosphorus main groups are located at 133 and 134.1 eV and correspond to C-P-O groups (such as C-$PO(OH)_2$ or C_2-PO(OH)) and to the C-O-P ones (C-O-$PO(OH)_2$ and $(C\text{-}O)_3PO$) respectively [1]. **Fig. 9a** shows the P2p spectra of the same electrode sample of ACP-N submitted to a mild and severe electro-reduction treatment studied above. An important decrease of P content compared to that of ACP can be observed (**Table 1**), mainly associated to the removal of C-O-$PO(OH)_2$ groups as H_3PO_4 during the preparation of ACP-N from ACP [25]. The mild electro-reduction treatment does not modify the P oxidation state. However, the severe one leads to a more reduced phosphorus species than those observed for ACP-N, which can be appreciated with a slight displacement of the peak to lower binding energies. This displacement can be due to the reduction of C-$PO(OH)_2$ groups to $C_2PO(OH)$, according to the mechanism proposed by Berenguer et al. [20].

By contrast, a more reduced species is observed in ACP-NB after the chemical reduction treatment from nitro to amino groups (**Fig. 9b**) [30]. In this case, a shift of the spectrum to a more oxidized phosphorus structure is observed after the electro-oxidation

treatment of the electrode. This can be probably due to the oxidation of $C_2PO(OH)$ structures to $C\text{-}PO(OH)_2$ [20]. On the contrary, XPS analyses does not show any change in the chemical state of P after the electro-oxidation treatment of ACP-E (**Fig. 9c**). These results are consistent with the modification of nitrogen structures during the electrochemical treatment and suggest a synergy between nitrogen and phosphorus surface groups[18].

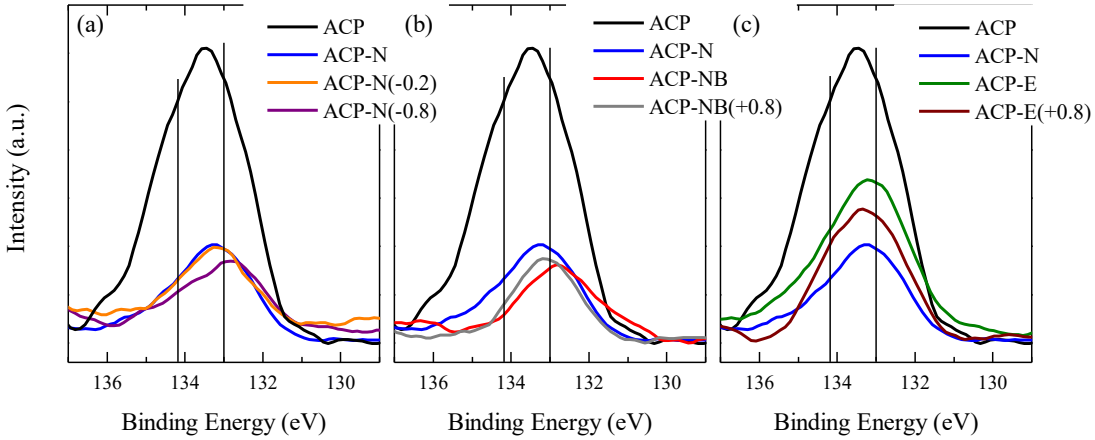

Fig. 9. P2p XPS spectra of (a) ACP-N, (b) ACP-NB and (c) ACP-E electrodes and their resulting electrodes after reduction and oxidation treatments.

According to our previous results on the active participation of P-groups in the oxygen introduction on the carbon surface [20], the formation of the hydroxylamine could probably be facilitated by the hydroxyl radical captor/donor character of these P-groups. Thereby, **Figure 10** shows the proposed electrochemical pathways, which could explain the modifications in the ACP-Ns carbon series surface registered by means of XPS. **Fig. 10a** shows the proposed amine electro-oxidation pathway through the formation of a hydroxylamine group. This hydroxylamine group could be associated to the new peak centered at ca. 402 eV in N1s spectrum for ACP-NB after electrooxidation treatment. On the other hand, the analogy of CV and XPS results obtained for ACP-N, compared to those obtained for ACP-NB, seems to indicate that the electro-reduction of nitro surface group could begin with the formation of a dihydroxylamine species through a proton transfer reaction from the acid electrolyte, forming this nitrogen compound on the carbon surface (**Fig. 9b**).

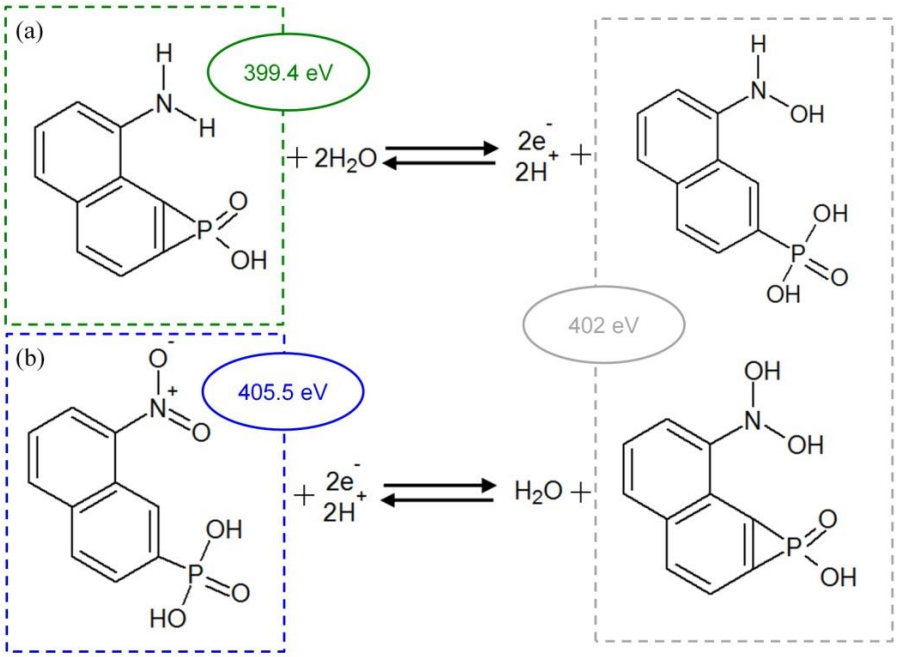

Fig. 10. Reaction pathways of (a) amine group electro-oxidation and (b) nitro group electro-reduction including the transformation of P-groups during the electrochemical processes

The formation of hydroxylamine structures could be related with the presence of peaks in the CV of the activated carbon, suggesting that these nitrogen groups are the electrochemically active ones. In this way, it is assumable that amino and nitro groups bonded to aromatic structures (probably in the vicinity of P-groups) of ACP are capable of forming the active species, whereas amides or aliphatic amine from amido-amine functionalization are not able. This hypothesis would explain the results obtained from ACP-E: (i) a rectangular CV shape, (ii) N1s spectrum of ACP-E is unchanged after an electro-oxidation treatment and (iii) ACP-E1 and ACP-E2 show surprisingly high surface capacitances due to the extraordinary conductivity of the polymeric nitrogen chain and not associated to changes on the nitrogen oxidation state.

In a previous work, we have observed the high electrochemical stability of phosphorus groups and the capability of acting as hydroxyl radicals captor/donor [20], which suggests that they could contribute to pseudocapacitive reactions by facilitating the ion transport. Others authors even highlighted the positive contribution of P-groups on N-doped activated carbon electrochemical performance [18,46,48]. In this sense, although the presence of phosphorus on the surface of the nitrogen-doped carbons cannot be

directly related to the enhancement of the pseudocapacitive behavior of carbons, it does indirectly due to: (i) phosphorus plays a key role on the selective incorporation of $–NO_2$ groups on the carbon surface [25]; (ii) also plays an important role in the selective reduction of $–NO_2$ to $–NH_2$ [30] and (iii) minor modifications in the phosphorus oxidation state are only appreciated in ACP-N and ACP-NB, in which the formation of hydroxylamino groups is proposed.

4. Conclusions

A large variety of nitrogen surface groups were prepared by different chemical and thermal treatments from a phosphorus-containing activated carbon. Their electrochemical performances have been studied and all of them have shown an enhancement of the activated carbon capacitance due to pseudocapacitive contributions.

Nitro and amine-containing activated carbons exhibit a typical pseudocapacitive behavior, showing considerable peaks in the cyclic voltammogram. These peaks could be related to the hydroxylamine formation reactions from the initial N-groups. The presence of condensed nitrogen structures (pyrrolic and pyridinic) in these activated carbon enhances the conductivity of the electrodes, enlarging the rectangular CV part of the voltammogram and achieving specific capacitances of 317 F g^{-1}. In addition these groups improve the electron transfer reactions on the carbon surface.

Poly(amido-amine)-containing activated carbons present an important amount of surface nitrogen concentration due to the large polymeric chains that causes the pore blockage. These carbons exhibit a surprisingly high surface capacitance (3256 mF m^{-2}) mainly due to the high-conductivity and the pseudocapacitive effect of the nitrogen chain. However, these carbons do not show modifications of the N oxidation state during the voltammetric analyses.

At last, quaternary nitrogen-containing activated carbons present a fast development of the electric double layer and exhibit a perfect box-like cyclic voltammogram (with specific capacities of 256 F g^{-1}). The presence of this specific nitrogen surface species and the more ordered carbon structure explain this result.

Acknowledgements

This work was supported by the Spanish Ministry of Economy and Competitiveness through CTQ2015-68654-R project.

References

[1] J. Bedia, R. Barrionuevo, J. Rodríguez-Mirasol, T. Cordero, Ethanol dehydration to ethylene on acid carbon catalysts, Appl. Catal. B Environ. 103 (2011) 302–310.

[2] I. Hita, T. Cordero-Lanzac, A. Gallardo, J.M. Arandes, J. Rodríguez-Mirasol, J. Bilbao, T. Cordero, P. Castaño, Phosphorus-containing activated carbon as acid support in a bifunctional Pt-Pd catalyst for tire oil hydrocracking, Catal. Commun. 78 (2016) 48–51.

[3] L.M. Cotoruelo, M.D. Marqués, A. Leiva, J. Rodríguez-Mirasol, T. Cordero, Adsorption of oxygen-containing aromatics used in petrochemical, pharmaceutical and food industries by means of lignin based active carbons, Adsorption. 17 (2011) 539–550.

[4] F.J. García-Mateos, R. Ruiz-Rosas, M.D. Marqués, L.M. Cotoruelo, J. Rodríguez-Mirasol, T. Cordero, Removal of paracetamol on biomass-derived activated carbon: Modeling the fixed bed breakthrough curves using batch adsorption experiments, Chem. Eng. J. 279 (2015) 18–30.

[5] F. Béguin, V. Presser, A. Balducci, E. Frackowiak, Carbons and electrolytes for advanced supercapacitors, Adv. Mater. 26 (2014) 2219–2251.

[6] Y. Zhai, Y. Dou, D. Zhao, P.F. Fulvio, R.T. Mayes, S. Dai, Carbon Materials for Chemical Capacitive Energy Storage, Adv. Mater. 23 (2011) 4828–4850.

[7] H. Wang, A.C. Forse, J.M. Griffin, N.M. Trease, L. Trognko, P.L. Taberna, P. Simon, C.P. Grey, In situ NMR spectroscopy of supercapacitors: Insight into the charge storage mechanism, J. Am. Chem. Soc. 135 (2013) 18968–18980.

[8] L. Sun, C. Tian, M. Li, X. Meng, L. Wang, R. Wang, J. Yin, H. Fu, From coconut shell to porous graphene-like nanosheets for high-power supercapacitors, J. Mater. Chem. A. 1 (2013) 6462–6470.

[9] D. Salinas-Torres, J.M. Sieben, D. Lozano-Castelló, D. Cazorla-Amorós, E. Morallón, Asymmetric hybrid capacitors based on activated carbon and activated carbon fibre-PANI electrodes, Electrochim. Acta. 89 (2013) 326–333.

[10] C.O. Ania, V. Khomenko, E. Raymundo-Piñero, J.B. Parra, F. Béguin, The large electrochemical capacitance of microporous doped carbon obtained by using a zeolite template, Adv. Funct. Mater. 17 (2007) 1828–1836.

[11] R. Ryoo, S.H. Joo, M. Kruk, M. Jaroniec, Ordered mesoporous carbons, Adv. Mater. 13 (2001) 677–681.

[12] K. Nueangnoraj, R. Ruiz-Rosas, H. Nishihara, S. Shiraishi, E. Morallón, D. Cazorla-Amorós, T. Kyotani, Carbon-carbon asymmetric aqueous capacitor by pseudocapacitive positive and stable negative electrodes, Carbon. 67 (2014) 792–794.

[13] D. Hulicova-Jurcakova, M. Seredych, G.Q. Lu, T.J. Bandosz, Combined effect of nitrogen- and oxygen-containing functional groups of microporous activated carbon on its electrochemical performance in supercapacitors, Adv. Funct. Mater. 19 (2009) 438–447.

[14] M. Zhong, E.K. Kim, J.P. McGann, S.E. Chun, J.F. Whitacre, M. Jaroniec, K. Matyjaszewski, T. Kowalewski, Electrochemically active nitrogen-enriched nanocarbons with well-defined morphology synthesized by pyrolysis of self-

assembled block copolymer, J. Am. Chem. Soc. 134 (2012) 14846–14857.
[15] M. Jagtoyen, F. Derbyshire, Activated carbons from yellow poplar and white oak by H3PO4 activation, Carbon. 36 (1998) 1085–1097.
[16] J.M. Rosas, R. Ruiz-Rosas, J. Rodríguez-Mirasol, T. Cordero, Kinetic study of the oxidation resistance of phosphorus-containing activated carbons, Carbon. 50 (2012) 1523–1537.
[17] L. Dai, D.W. Chang, J.-B. Baek, W. Lu, Carbon nanomaterials for advanced energy conversion and storage., Small. 8 (2012) 1130–66.
[18] D. Hulicova-Jurcakova, M. Seredych, G.Q. Lu, N.K.A.C. Kodiweera, P.E. Stallworth, S. Greenbaum, T.J. Bandosz, Effect of surface phosphorus functionalities of activated carbons containing oxygen and nitrogen on electrochemical capacitance, Carbon. 47 (2009) 1576–1584.
[19] U.B. Nasini, V.G. Bairi, S.K. Ramasahayam, S.E. Bourdo, T. Viswanathan, A.U. Shaikh, Phosphorous and nitrogen dual heteroatom doped mesoporous carbon synthesized via microwave method for supercapacitor application, J. Power Sources. 250 (2014) 257–265.
[20] R. Berenguer, R. Ruiz-Rosas, A. Gallardo, D. Cazorla-Amorós, E. Morallón, H. Nishihara, T. Kyotani, J. Rodríguez-Mirasol, T. Cordero, Enhanced electro-oxidation resistance of carbon electrodes induced by phosphorus surface groups, Carbon. 95 (2015) 681–689.
[21] D. Hulicova, J. Yamashita, Y. Soneda, H. Hatori, M. Kodama, Supercapacitors prepared from melamine-based carbon, Chem. Mater. 17 (2005) 1241–1247.
[22] H. Sun, L. Cao, L. Lu, Bacteria promoted hierarchical carbon materials for high-performance supercapacitor, Energy Environ. Sci. 5 (2012) 6206.
[23] Z. Li, Z. Xu, H. Wang, J. Ding, B. Zahiri, C.M.B. Holt, X. Tan, D. Mitlin, Colossal pseudocapacitance in a high functionality–high surface area carbon anode doubles the energy of an asymmetric supercapacitor, Energy Environ. Sci. 7 (2014) 1708.
[24] Y. Tang, B.L. Allen, D.R. Kauffman, A. Star, Electrocatalytic activity of nitrogen-doped carbon nanotube cups, J. Am. Chem. Soc. 131 (2009) 13200–13201.
[25] J.J. Ternero-Hidalgo, J.M. Rosas, J. Palomo, M.J. Valero-Romero, J. Rodríguez-Mirasol, T. Cordero, Functionalization of activated carbons by HNO3 treatment: Influence of phosphorus surface groups, Carbon. 101 (2016) 409–419.
[26] D.W. Wang, F. Li, L.C. Yin, X. Lu, Z.G. Chen, I.R. Gentle, G.Q. Lu, H.M. Cheng, Nitrogen-doped carbon monolith for alkaline supercapacitors and understanding nitrogen-induced redox transitions, Chem. - A Eur. J. 18 (2012) 5345–5351.
[27] D. Hulicova-Jurcakova, M. Kodama, S. Shiraishi, H. Hatori, Z.H. Zhu, G.Q. Lu, Nitrogen-enriched nonporous carbon electrodes with extraordinary supercapacitance, Adv. Funct. Mater. 19 (2009) 1800–1809.
[28] W. Ding, Z. Wei, S. Chen, X. Qi, T. Yang, J. Hu, D. Wang, L.J. Wan, S.F. Alvi, L. Li, Space-confinement-induced synthesis of pyridinic- and pyrrolic-nitrogen-doped graphene for the catalysis of oxygen reduction, Angew. Chem. Int. Ed. 52 (2013) 11755–11759.
[29] M.J. Mostazo-López, R. Ruiz-Rosas, E. Morallón, D. Cazorla-Amorós, Generation of nitrogen functionalities on activated carbons by amidation reactions and Hofmann rearrangement: Chemical and electrochemical characterization, Carbon. 91 (2015) 252–265.
[30] J. Palomo, J.J. Ternero-Hidalgo, J.M. Rosas, J. Rodríguez-Mirasol, T. Cordero,

Selective nitrogen functionalization of phosphorus-containing activated carbons, Fuel Process. Technol. 156 (2017) 438–445.
[31] J. Bedia, R. Ruiz-Rosas, J. Rodríguez-Mirasol, T. Cordero, Kinetic Study of the Decomposition of 2-Butanol on Carbon-Based Acid Catalyst, AIChe J. 56 (2010) 1557–1568.
[32] S. Moore, W.H. Stein, A modified ninhydrin reagent for the photometric determination of amino acids and related compounds, J. Biol. Chem. 211 (1954) 907–913.
[33] J.R. Pels, F. Kapteijn, J.A. Moulijn, Q. Zhu, K.M. Thomas, Evolution of nitrogen functionalities in carbonaceous materials during pyrolysis, Carbon. 33 (1995) 1641–1653.
[34] I. Martin-Gullon, J.P. Marco-Lozar, D. Cazorla-Amorós, A. Linares-Solano, Analysis of the microporosity shrinkage upon thermal post-treatment of H3PO4 activated carbons, Carbon. 42 (2004) 1333–1337.
[35] J. Bedia, J.M. Rosas, J. Rodríguez-Mirasol, T. Cordero, Pd supported on mesoporous activated carbons with high oxidation resistance as catalysts for toluene oxidation, Appl. Catal. B Environ. 94 (2010) 8–18.
[36] V.K. Sarin, S.B.H. Kent, J.P. Tam, R.B. Merrifield, Quantitative monitoring of solid-phase peptide synthesis by the ninhydrin reaction, Anal. Biochem. 117 (1981) 147–157.
[37] E. Gonzalez-Serrano, T. Cordero, J. Rodriguez-Mirasol, L. Cotoruelo, J.J. Rodriguez, Removal of water pollutants with activated carbons prepared from H 3PO4 activation of lignin from kraft black liquors, Water Res. 38 (2004) 3043–3050.
[38] X. Wu, L.R. Radovic, Inhibition of catalytic oxidation of carbon/carbon composites by phosphorus, Carbon. 44 (2006) 141–151.
[39] M.J. Bleda-Martínez, J.A. Maciá-Agulló, D. Lozano-Castelló, E. Morallón, D. Cazorla-Amorós, A. Linares-Solano, Role of surface chemistry on electric double layer capacitance of carbon materials, Carbon. 43 (2005) 2677–2684.
[40] R. Berenguer, F.J. García-Mateos, R. Ruiz-Rosas, D. Cazorla-Amorós, E. Morallón, J. Rodríguez-Mirasol, T. Cordero, Biomass-derived binderless fibrous carbon electrodes for ultrafast energy storage, Green Chem. 18 (2016) 1506–1515.
[41] F.J. García-Mateos, T. Cordero-Lanzac, R. Berenguer, E. Morallón, D. Cazorla-Amorós, J. Rodríguez-Mirasol, T. Cordero, Lignin-derived Pt supported carbon (submicron)fiber electrocatalysts for alcohol electro-oxidation, Appl. Catal. B Environ. 211 (2017) 18–30.
[42] K. Kierzek, E. Frackowiak, G. Lota, G. Gryglewicz, J. Machnikowski, Electrochemical capacitors based on highly porous carbons prepared by KOH activation, Electrochim. Acta. 49 (2004) 515–523.
[43] X. Wang, G. Sun, P. Routh, D.-H. Kim, W. Huang, P. Chen, Heteroatom-doped graphene materials: syntheses, properties and applications, Chem. Soc. Rev. 43 (2014) 7067–7098.
[44] M. Seredych, D. Hulicova-Jurcakova, G.Q. Lu, T.J. Bandosz, Surface functional groups of carbons and the effects of their chemical character, density and accessibility to ions on electrochemical performance, Carbon. 46 (2008) 1475–1488.
[45] M.J. Bleda-Martínez, D. Lozano-Castelló, E. Morallón, D. Cazorla-Amorós, A. Linares-Solano, Chemical and electrochemical characterization of porous carbon materials, Carbon. 44 (2006) 2642–2651.

[46] V. V. Strelko, V.S. Kuts, P.A. Thrower, On the mechanism of possible influence of heteroatoms of nitrogen, boron and phosphorus in a carbon matrix on the catalytic activity of carbons in electron transfer reactions, Carbon. 38 (2000) 1499–1503.

[47] S. Zhang, P. Kang, S. Ubnoske, M.K. Brennaman, N. Song, R.L. House, J.T. Glass, T.J. Meyer, Polyethylenimine-Enhanced Electrocatalytic Reduction of CO2 to Formate at Nitrogen-Doped Carbon Nanomaterials, J. Am. Chem. Soc. 136 (2014) 7845–7848.

[48] X. Yan, Y. Liu, X. Fan, X. Jia, Y. Yu, X. Yang, Nitrogen/phosphorus co-doped nonporous carbon nanofibers for high-performance supercapacitors, J. Power Sources. 248 (2014) 745–751.

[49] R. Pietrzak, XPS study and physico-chemical properties of nitrogen-enriched microporous activated carbon from high volatile bituminous coal, Fuel. 88 (2009) 1871–1877.

[50] E. Frackowiak, Carbon materials for supercapacitor application., Phys. Chem. Chem. Phys. 9 (2007) 1774–1785.

[51] W. Li, D. Chen, Z. Li, Y. Shi, Y. Wan, J. Huang, J. Yang, D. Zhao, Z. Jiang, Nitrogen enriched mesoporous carbon spheres obtained by a facile method and its application for electrochemical capacitor, Electrochem. Commun. 9 (2007) 569–573.